A Human Liver-on-a-Chip Platform for Modeling Nonalcoholic Fatty Liver Disease

Soufian Lasli, Han-Jun Kim, KangJu Lee, Ceri-Anne E. Suurmond, Marcus Goudie, Praveen Bandaru, Wujin Sun, Shiming Zhang, Niyuan Zhang, Samad Ahadian, Mehmet R. Dokmeci, Junmin Lee,* and Ali Khademhosseini*

The liver possesses a unique microenvironment with a complex internal vascular system and cell–cell interactions. Nonalcoholic fatty liver disease (NAFLD) is the most common form of chronic liver disease, and although much effort has been dedicated to building models to target NAFLD, most in vitro systems rely on simple models failing to recapitulate complex liver functions. Here, an in vitro system is presented to study NAFLD (steatosis) by coculturing human hepatocellular carcinoma (HepG2) cells and umbilical vein endothelial cells (HUVECs) into spheroids. Analysis of colocalization of HepG2–HUVECs along with the level of steatosis reveals that the NAFLD pathogenesis could be better modeled when 20% of HUVECs are presented in HepG2 spheroids. Spheroids with fat supplements progressed to the steatosis stage on day 2, which could be maintained for more than a week without being harmful for cells. Transferring spheroids onto a chip system with an array of interconnected hexagonal microwells proves helpful for monitoring functionality through increased albumin secretions with HepG2–HUVEC interactions and elevated production of reactive oxygen species for steatotic spheroids. The reversibility of steatosis is demonstrated by simply stopping fat-based diet or by antisteatotic drug administration, the latter showing a faster return of intracellular lipid levels to the basal level.

1. Introduction

The liver is the largest organ in individuals representing 2–5% of total adult weight. The main function of the liver, as part of the digestive system, is to filter blood coming from the digestive tract through transformation, detoxification, and accumulation of metabolites (nutrients as well as xenobiotics). The liver also plays an important role in carbohydrate metabolism, production of plasma proteins such as albumin, and regulating components of the bile such as bile acids. It possesses a unique microenvironment with a complex internal vascular system and multiple cell–cell interactions between hepatocytes, sinusoidal endothelial, Kupffer, and stellate cells.[1,2] These multiple cell types existing in the liver niche function as an integral unit, and their communications through direct contact and diffusible signals enable the homeostatic processes of the liver.

S. Lasli, Dr. H.-J. Kim, Dr. K. Lee, C. E. Suurmond, Dr. M. Goudie,
P. Bandaru, Dr. W. Sun, Dr. S. Zhang, N. Zhang, Dr. S. Ahadian,
Dr. J. Lee, Prof. A. Khademhosseini
Department of Bioengineering
Henry Samueli School of Engineering and Applied Sciences
University of California—Los Angeles
Los Angeles, CA 90095, USA
E-mail: junmin@ucla.edu; khademh@ucla.edu
S. Lasli, Dr. H.-J. Kim, Dr. K. Lee, C. E. Suurmond, Dr. M. Goudie,
P. Bandaru, Dr. W. Sun, Dr. S. Zhang, N. Zhang, Dr. S. Ahadian,
Prof. M. R. Dokmeci, Dr. J. Lee, Prof. A. Khademhosseini
Center for Minimally Invasive Therapeutics
University of California—Los Angeles
Los Angeles, CA 90095, USA
S. Lasli
Institute of Bioengineering
School of Life Sciences and School of Engineering
Ecole Polytechnique Fédérale de Lausanne
1015 Lausanne, Switzerland

C. E. Suurmond
Bioengineering Technologies
University of Twente
7522 NB Enschede, The Netherlands
N. Zhang
College of Chemistry
Nankai University
Tianjin 300071, China
Prof. M. R. Dokmeci, Prof. A. Khademhosseini
Department of Radiology
David Geffen School of Medicine
University of California—Los Angeles
Los Angeles, CA 90095, USA
Prof. A. Khademhosseini
Department of Chemical and Biomolecular Engineering
Henry Samueli School of Engineering and Applied Sciences
University of California—Los Angeles
Los Angeles, CA 90095, USA

**ADVANCED
SCIENCE NEWS**
www.advancedsciencenews.com

**ADVANCED
BIOSYSTEMS**
www.adv-biosys.com

Nonalcoholic fatty liver disease (NAFLD), the most common form of chronic liver disease, affects 20–50% of people[3] and has been predicted to be the major cause of liver failure as well as a leading indication for liver transplantation once progressed into severe form such as nonalcoholic steatohepatitis (NASH).[4] The disease is caused by the imbalance of diverse complex processes, including lipolysis, triglyceride synthesis, very low density lipoprotein secretion, de novo lipogenesis, and oxidation, leading to abnormal accumulation of fat in the form of triglycerides in hepatocytes.[5] The putative steps of NAFLD involve 1) NAFL where lipid accumulates in hepatocytes (steatosis) without signs of injury,[6] 2) NASH where inflammation occurs, 3) fibrosis where excessive collagen is deposited, and 4) cirrhosis, hepatocellular carcinoma, and liver-related mortality.[3,4,6–8] Although NAFLD possesses a high prevalence, more than 90% of the patients only get simple steatosis that is not related to impaired survival. Approximately 5–10% of subjects develop NASH and among them 30% develop cirrhosis.[7] Despite the gravity of the situation, no effective therapy exists.[8] However, bioengineering strategies to recapitulate the complex liver cell niche may hold promise for facilitating the development of NAFLD-targeted drugs.

Several models of NAFLD exist including both animal and in vitro systems. Nonetheless, current dietary, genetic, or chemically manipulated animal models do not accurately reflect the multifactorial, integrated steps in NAFLD human pathology and disease progression.[9–12] Microengineered cell culture models, particularly organs-on-a-chip systems, could address the limitations of animal models due to the use of human cells cultured in a 3D environment.[13] For example, Gori et al. investigated NAFLD pathogenesis on a liver-on-a-chip.[14] Their chip consisted of a cord of hepatocytes cultured in a grid of closely spaced and parallel microchannels mimicking the endothelial–parenchymal interface of a liver sinusoid, but actual endothelial cells were not employed to build the system. Other studies by Kozyra et al. and Cordero-Herrera et al. reported a human hepatic 3D spheroid system using primary human hepatocytes (PHHs) capable of mimicking steatosis conditions in a reversible manner and to prevent steatosis by a simple dietary approach, respectively.[15,16] In addition, Kostrzewski et al. developed a 3D perfused platform using PHHs for steatosis evaluation involving 12 isolated bioreactors where each one has its own flow rate generating an oxygen gradient across the tissue reproducing the in vivo liver sinusoid zonation.[17] Furthermore, a multiorgan (gut–liver) system was reported by Lee and Sung recapitulating the process of absorption and metabolism of lipids by the gut (Caco-2 cells), which were subsequently deposited within liver cells (HepG2). The effect of butyrate, tumor necrosis factor-α, and α-lipoic acid as molecules affecting steatosis was evaluated.[18] However, these platforms only focused on hepatocytes while skipping the importance of their interactions with nonparenchymal cells (NPCs), which may fail to recapitulate the complex hepatic microenvironment for modeling NAFLD.

Coculturing hepatocytes with NPCs could add a level of complexity resulting in a better mimicking of the in vivo hepatic lobule. Indeed, inclusion of NPCs in hepatic culture systems has been shown to enhance hepatocyte biosynthetic functions and metabolic response to drug treatment.[19] For instance, sinusoidal endothelial cells—important for vascularization—improved functionality of hepatocytes such as cytochrome P450 (CYP450) activity and albumin secretion, providing optimal trophic support for the hepatocytes.[19,20] Another study by Ehrlich et al. developed a sensor-integrated liver on chip array using human liver organoids composed of albumin-positive E6/E7LOW hepatocytes and endothelial cells, monitoring oxygen while glucose, lactate, and temperature were measured in real time using microfluidic electrochemical sensors. Although the study showed that lipid accumulation is not a result of increased production but rather suppression of fatty acid oxidation, their platform did not focus on steatosis.[21] An in vitro liver model was engineered by Feaver et al. by coculturing PHHs, hepatic stellate cells, and macrophages. The system incorporated hemodynamic flow along with lipotoxic stress risk factors including fatty acids, glucose, and insulin to induce and study NASH. They compared their results with NASH patients and found key similarities between their in vitro model and in vivo. However, physical interactions between different cell types were not incorporated since PHHs were separated from the other cell types by a synthetic membrane.[22]

Multicellular spheroids have many advantages over simple coculture of cells in 2D, allowing to create gradients in nutrients, metabolites, catabolites, and oxygen in the radial direction.[23] This is particularly important for the liver since the in vivo hepatic lobule presents an oxygen gradient, and thus, the use of spheroids for constructing the native liver tissue in vitro might improve the cellular functionality as well as the response for drug toxicity assessment.[24] Here, a bioengineered liver steatosis model was developed based on the interactions between human hepatocytes (HepG2) and primary human endothelial cells (HUVECs) by forming multicellular aggregates to investigate steatosis pathogenesis. Moreover, the spheroids composed of HepG2 cells and HUVECs were transferred onto a chip platform to establish a steatosis disease-on-a-chip model that can be used for monitoring of hepatocyte functionality and the development of a pharmaceutical tool to evaluate new potential drugs.

2. Results and Discussion

2.1. HepG2 Spheroid Formation and Their Size Optimization

The hepatic microenvironment with its multiple cell–cell interactions and complex internal vascular system plays a crucial role in maintaining liver homeostasis. In addition, compared to 2D culture systems, 3D cell spheroids are building units for tissue engineering and regenerative medicine due to their unique structure with direct cell–cell contacts. To build a 3D in vitro hepatic system using multicellular spheroids composed of HepG2 and HUVECs, AggreWell™400 culture plates were employed for the formation of spheroids. These multicellular spheroids were collected and transferred onto a chip system containing an array of interconnected hexagonal microwells that mimic the human liver organization. This chip system may be used as a platform to model steatosis by recapitulating the main symptoms encountered in vivo and assess specific biomarkers in response to drugs (**Figure 1**A). Each of the 1200 microwells that compose each well of the culture plate
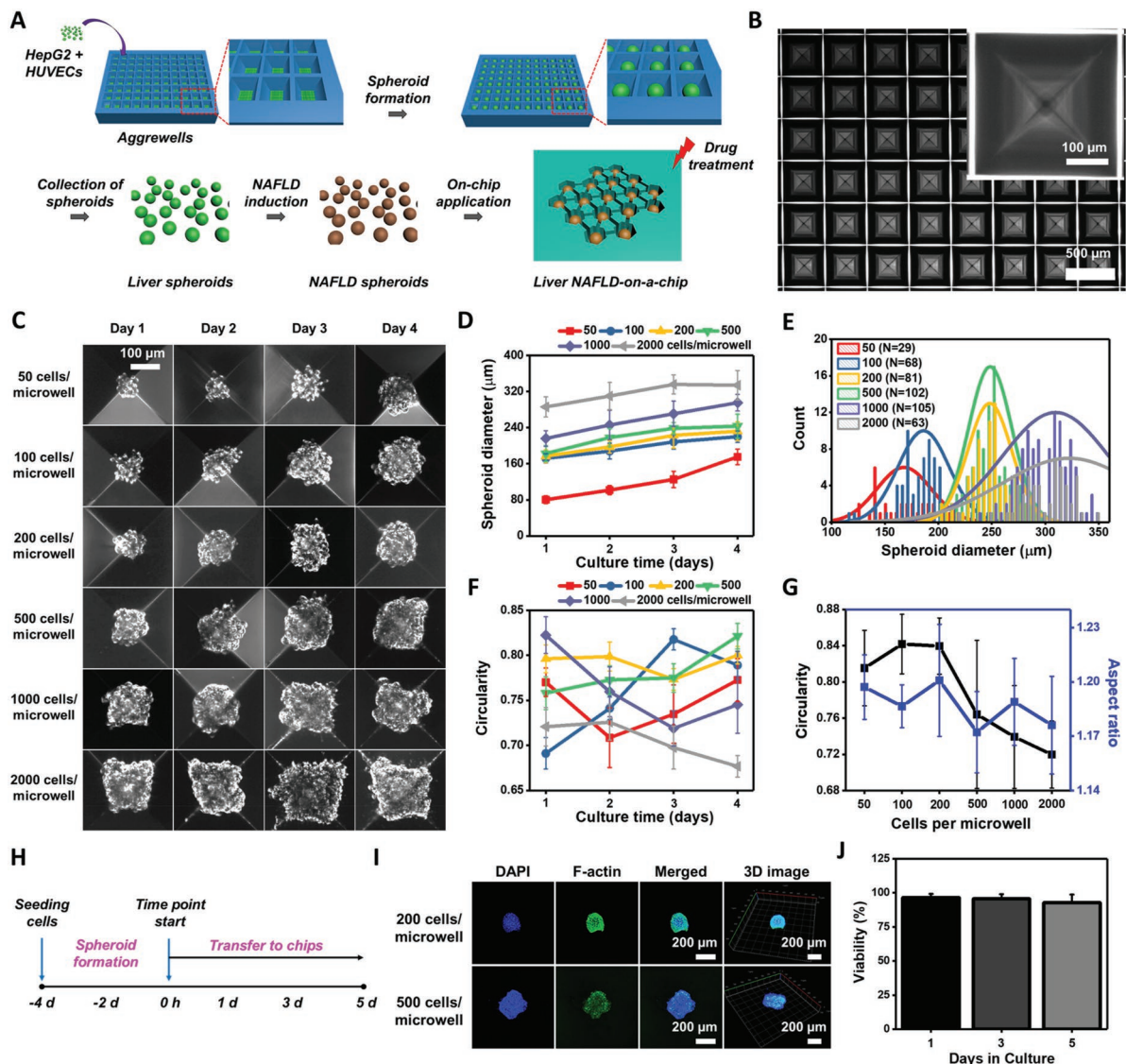
**ADVANCED
SCIENCE NEWS**
www.advancedsciencenews.com

**ADVANCED
BIOSYSTEMS**
www.adv-biosys.com

Figure 1. Formation of spheroids in the inverted pyramid-shaped microwells and their size selection. A) Schematic displaying the development of NAFLD-on-a-chip platform using bioengineered liver tissue spheroids comprised of two main cell types (HepG2 and HUVECs). B) A photograph of inverse pyramidal microwells with a diameter of 400 µm. C) HepG2 spheroids cultured for 4 days in the inverse pyramidal microwells. D) Quantification of spheroid size over the culture time in the inverted pyramid-shaped microwells with different initial seeding densities. E) Histogram of the spheroid diameters across the conditions after collecting them from the inverted pyramid-shaped microwells. F) Circularity of spheroids in the inverted pyramid-shaped microwells over 4 days. G) Comparison between circularity and aspect ratio of spheroids after harvesting them from the inverse pyramidal microwells. H) The timeline for the experiments. When spheroids were cultured for 4 days in the inverse pyramidal microwells and transferred into the microchip platform or multiwell plates, it was considered as the experiment starting point. I) Representative immunofluorescence images of F-actin/DAPI staining of spheroids on day 1 after collecting spheroids. J) Viability of cells in spheroids cultured for 1, 3, and 5 days based on the timeline ($N = 3$). Error bars represent standard deviation.

(24 wells) possesses an inverse pyramidal shape with a diameter of 400 µm, allowing high-throughput spheroid formation (Figure 1B). Furthermore, by seeding different cell densities (50, 100, 200, 500, 1000, and 2000 cells per microwell), the spheroid size can be easily tuned (Figure 1C).

Several characteristics of spheroids such as the diameter, circularity, and aspect ratio were assessed as functions of the initial cell concentration during the spheroid formation (Figure 1D–G). It is known that the diameter of spheroids is critical because large spheroids show necrosis in the core due

to hypoxia. An ideal size of spheroids is reported as around 200–300 µm in diameter where cell functionality is preserved while avoiding the necrotic core.[24] However, a previous study about HepG2 spheroids demonstrated that liver spheroids with the size of 400 µm did not possess a visible necrotic core but started to express elevated levels of necrotic biomarkers once the size of 700 µm was reached.[25] Circularity is also an important feature for liver spheroids because a linear gradient of oxygen tension should be ensured as it is the case in the real liver microarchitecture; in fact, the liver sinusoids could

be separated in different zones (high oxygen tension in the periphery and low in the center), which is crucial for the organ homeostasis.[26,27] We found that the initial concentrations of around 100, 200, and 500 cells per microwell led to the spheroid sizes of ≈220 ± 12, ≈232 ± 20, and ≈243 ± 26 µm, respectively (Figure 1D). Below 100 cells per microwell, the spheroid size was too small, while above 500 cells per microwell the size was too big to be employed for studying NAFLD pathogenesis. The size distribution histogram showed that the final size of spheroids after harvesting was uniform for the initial concentrations of 100, 200, and 500 cells per microwell (Figure 1E). The circularity evolution of spheroids cultured for 4 days in the inverted pyramid-shaped microwells suggests that the seeding densities of 100, 200, and 500 cells per microwell would be better for maintaining and developing the circularity compared to the other conditions with less and more initial seeding densities (Figure 1F). The aspect ratio is also an important parameter to characterize protrusions as it was observed due to the inverse pyramidal microwells (Figure S1, Supporting Information). As mentioned earlier, the circularity is linked to the linear gradient of oxygen tension; thus, spheroids possessing both the high circularity and low aspect ratio are desirable to optimize their size. Based on the analysis of circularity and aspect ratio of harvested spheroids, we selected the best conditions as being 100 and 200 cells per microwell since they displayed values of ≈0.84 and ≈0.81 for circularity and ≈1.19 and ≈1.2 for the aspect ratio, respectively (Figure 1G).

Spheroids cultured for 4 days in the inverse pyramidal microwells were harvested and transferred into either polydimethylsiloxane (PDMS) chips or multiwell plates for further characterization (experiment starting point) (Figure 1H). F-actin/4′,6-diamidino-2-phenylindole dihydrochloride (DAPI) staining was performed on day 5 to observe the structure of spheroids. With the initial condition of 200 cells per microwell, we observed a homogeneous distribution of the actin molecules between cells within the whole spheroids, demonstrating strong cell–cell interactions (Figure 1I). In addition, we observed a better morphology of spheroids for the condition of 200 cells per microwell compared to that of 500 cells per microwell, reinforcing the selection of this initial concentration. We further performed a live/dead assay of HepG2 spheroids (200 cells per microwell) that have been cultured for 4 days in the inverse pyramidal microwells and then transferred onto multiwell plates. The spheroids showed a viability of ≈92%, indicating that spheroids could be transferred without significant damages (Figure 1J). Taken together, we decided to pursue the rest of the experiments using 200 cells per microwell as the initial condition due to the suitable spheroid size (≈232 µm), uniform size distribution, and excellent combination of circularity/aspect ratio.

2.2. Colocalization of HepG2 and HUVECs in Spheroids

In this study, we hypothesized that bioengineering strategies to recapitulate the complex liver cell niche by coculturing HepG2 and HUVECs as spheroids may provide 1) the promotion of vascularization of HUVECs and 2) the improvement of functionality of HepG2 cells to build a steatosis disease model-on-a-chip system for modeling NAFLD. To test this hypothesis, HepG2 and HUVECs were mixed at different ratios (0%, 10%, 20%, and 30% of HUVECs with 100%, 90%, 80%, and 70% of HepG2, respectively, with the total initial cell number of ≈200 cells as previously set) and cultured for 4 days in the inverse pyramidal microwells. Then, we investigated the repartition and colocalization of two cell types as a function of the HepG2–HUVEC ratio. A 3D cell tracking technique was used to visualize HepG2 (red) and HUVECs (green) inside multicellular spheroids (**Figure 2**A). First, we assessed the approximate fraction of HUVECs after transferring to multiwell plates, showing that the measured values of 15 ± 4%, 21 ± 4%, and 27 ± 12% were comparable to the theoretical values of 10%, 20%, and 30%, respectively (Figure 2B). Next, we examined the effect of HepG2–HUVEC ratio on the colocalization of HepG2 and HUVECs within the spheroids (Figure 2C,D). We found that a higher number of HepG2 cells were localized in close proximity to HUVECs, and the percentage of HepG2–HUVEC colocalization was higher in spheroids where 10% of HUVECs were mixed with 90% of HepG2 cells compared to the colocalization percentages for 20% (≈1.15-fold) and 30% (≈1.26-fold) of HUVECs in spheroids (Figure 2C). These results suggest that a lower HUVEC population in spheroids may have higher chance to be surrounded by HepG2 cells, which strengthens cell–cell interaction between the two cell types compared to spheroids made of a higher HUVEC concentration. Then, we further assessed the 3D distribution of HUVECs using a confocal microscope by dividing spheroids into three different sections (Figure 2E). We noticed that most of HUVECs were located in the middle section of the spheroids (section 2) and distributed equally within the plane, which is in agreement with a previous report showing that the outward HUVEC migration to the edges of spheroids was hindered in our cell culture condition with the supplement of vascular endothelial growth factor in the HUVEC medium.[23]

2.3. Steatosis Induction and Optimized Ratio for HepG2–HUVECs

To examine whether spheroids with different ratios of HepG2 and HUVECs could take up lipids differently after exposure to free fatty acids (FFAs), we supplemented liver FFAs (palmitic acid (PA): 0.33×10^{-3} M; oleic acid (OA): 0.66×10^{-3} M) in the cell culture medium for 2 days to induce hepatic steatosis in harvested spheroids as described previously (**Figure 3**A).[14] In order to facilitate the uptake of lipids by HepG2 cells, 1% bovine serum albumin (BSA) was added into the cell culture medium.[28] It is well known that hepatocytes can absorb supplemented lipids that will be accumulated in the cytoplasm in the form of droplets; fortunately, the early stage of clinical hepatic steatosis could be reversed by simply changing a lifestyle such as having a healthy diet and exercise to accomplish weight loss (Figure 3B).[29] Intracellular lipid accumulation was investigated using an AdipoRed assay in both 2D and 3D HepG2–HUVEC cocultures (Figure 3C–I). For the 2D coculture, 20 000 cells were seeded into 24-well plates, and steatosis was induced for 2 days in fatty acid media after the overnight culture in healthy media (Figure 3C). Cells cultured in fatty acid media displayed
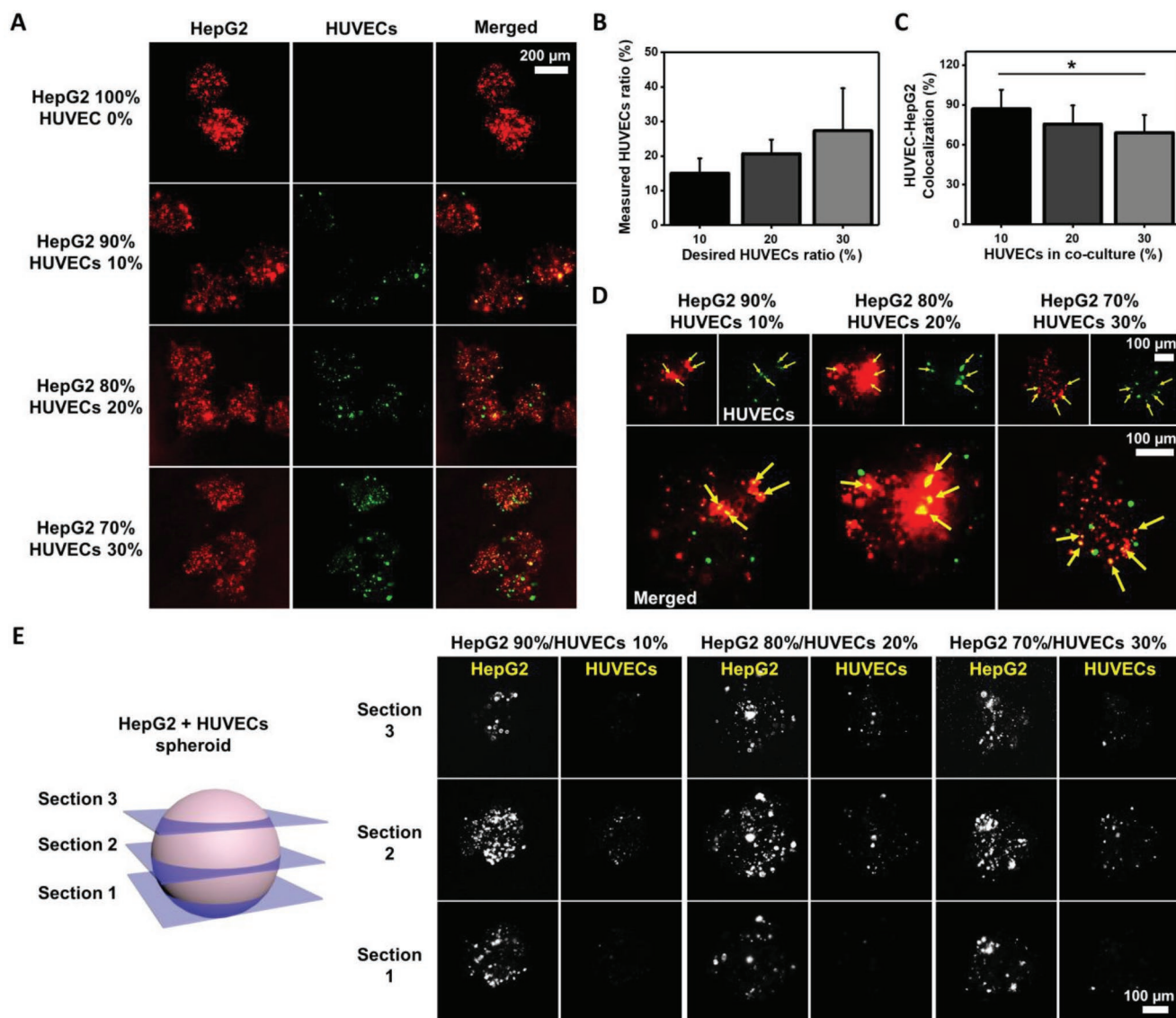
Figure 2. Coculture of HepG2 and HUVECs in spheroids and study of their colocalization. A) Representative confocal images of spheroids composed of HepG2 (red) and HUVECs (green) with different ratios. B) Measured fraction of HUVECs in HepG2 spheroids with desired ratio of 10%, 20%, and 30% ($N = 3$). C) Percentage of HepG2–HUVEC colocalization in 10%, 20%, and 30% HUVEC spheroids ($N = 8$ for 10%, $N = 6$ for 20%, and $N = 14$ for 30%). D) Representative confocal images showing colocalization of HepG2 and HUVECs. Overlapped cells between HepG2 and HUVECs (yellow) in the focal plane were marked with yellow arrows. E) Schematic representing three different sections of HepG2–HUVEC spheroids and representative confocal images of HepG2 and HUVECs with different ratios at each section. *$P < 0.05$, Student's t-test. Error bars represent standard deviation.

higher levels of accumulated lipids for 0% (≈2.54-fold), 10% (≈2.27-fold), and 20% (≈2.09-fold) of HUVECs in 2D culture compared to those cultured in the healthy medium (Figure 3D). Interestingly, we also found that the 2D culture with 30% of HUVECs and 70% of HepG2 cells exhibited nonsignificant changes (≈1.26-fold higher than control). To ensure that FFAs have no effect on HUVECs, we assessed the lipid accumulation level in HUVECs cultured with or without the supplement of FFAs (Figure 3E,F). The results displayed that the lipid accumulation was not observed in HUVECs, suggesting that the hepatic steatosis development only occurred in HepG2 cells.

To validate the observed trends of lipid accumulation in 2D cultures, we performed the same assay in a 3D configuration.

Unlike the 2D results of lipid accumulation, we found a slight increase in intracellular lipid accumulation when increasing the ratio of HUVECs in spheroids (Figure 3G,H). These results suggest that multicellular spheroids offer better representation of in vivo–like structures as they provide an ideal 3D environment with the cell–cell interactions through tight junctions. Since accumulated lipids are known to form droplets inside cells, we further quantified the level of lipid droplets in spheroids using a confocal microscope (Figure 3I,J). The area of lipid droplets was normalized by the area of each spheroid to compare the levels of lipid accumulation across the different conditions (Figure S2, Supporting Information). The results exhibited that the lipid area over the total surface
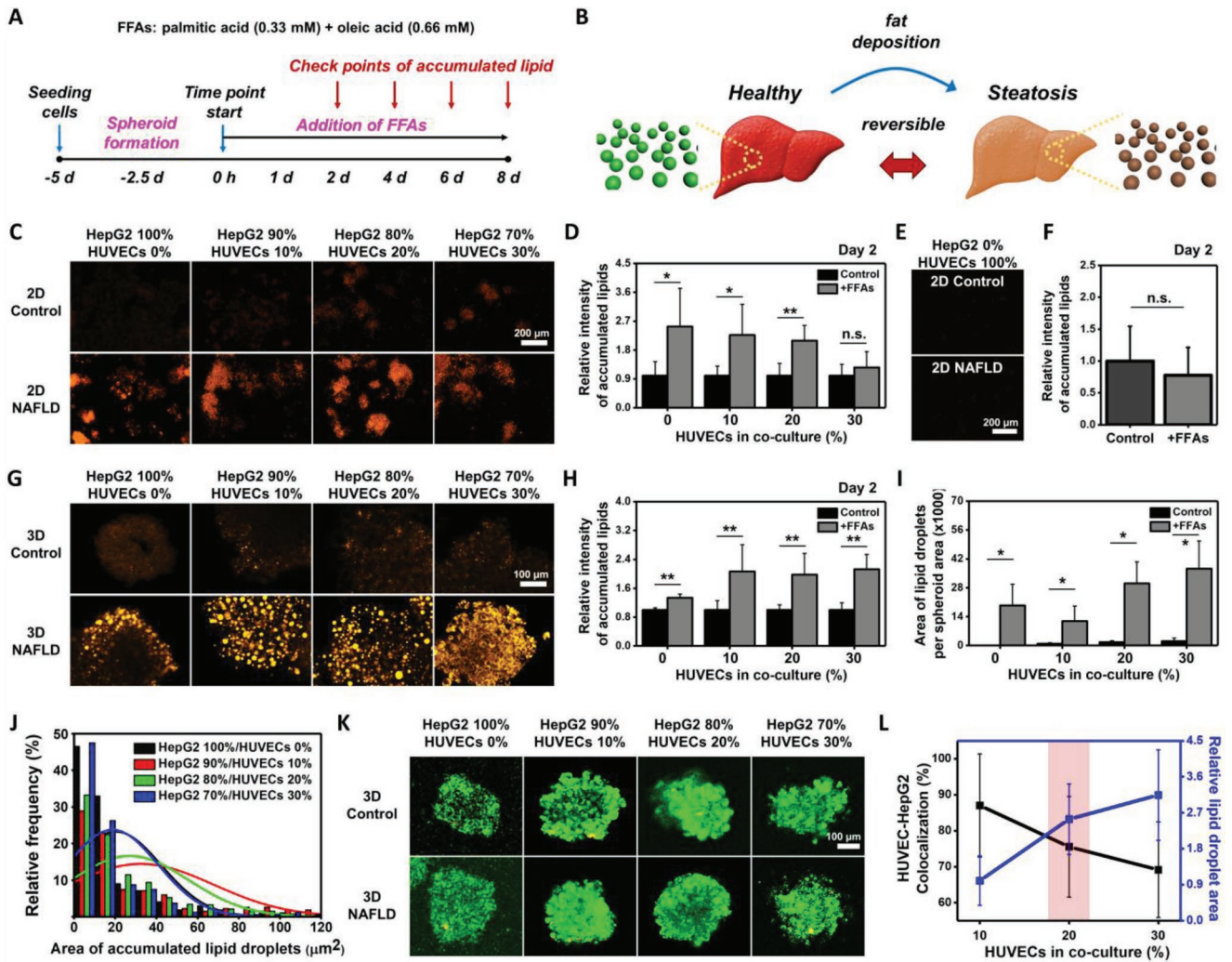
Figure 3. Steatosis induction in spheroids with different HepG2–HUVEC ratios and optimization of their fraction. A) The timeline for steatosis induction. Spheroids formed for 4 days in the inverted pyramid-shaped microwells were transferred and cultured in multiwell plates overnight before the addition of FFAs in the cell culture medium. B) Schematic exhibiting fatty acids could be accumulated inside hepatocytes (steatosis) and the process could be reversible. C) Representative immunofluorescence images and D) quantification of accumulated lipids in HepG2 cultured for 2 days on 2D system with different ratios of HUVECs ($N = 4$). E) Representative immunofluorescence images and F) quantification of accumulated lipids in HUVECs on 2D system ($N = 4$). G) Representative immunofluorescence images of accumulated lipids on day 2 showing intracellular lipid accumulation in 3D system. H) Quantitation of the relative intensity of intracellular lipids in the 3D system ($N > 4$ for each condition). I) Area of lipid droplets per spheroid area as a function of the HUVEC percentage in coculture in 3D system (normalized to HepG2 fraction). J) Histogram of the accumulated lipid droplet area across the conditions. K) Representative immunofluorescence images of live/dead staining for cells in spheroids after 2 days of steatosis induction. L) Comparison between HepG2–HUVEC colocalization and relative droplet area as a function of the HUVEC percentage in coculture to optimize the fraction of HepG2–HUVECs in spheroids. $*P < 0.05$, $**P < 0.005$, Student's t-test. Error bars represent standard deviation.

increased with increasing population of HUVECs in spheroids with a maximum at the 30% HUVECs/70% HepG2 cell ratio; the lipid area of spheroids containing 30% HUVECs was ≈1.92-fold, ≈3.14-fold, and ≈1.24-fold higher compared to 0%, 10%, and 20% of HUVECs in spheroids, respectively (Figure 3I; Figure S3, Supporting Information). A histogram representing the area of accumulated lipid droplets in spheroids as a function of HUVEC ratio was produced, displaying the formation of smaller droplets in spheroids composed of 0% and 30% of HUVECs relative to 10% and 20% where bigger droplets were found with a wider range of lipid area (Figure 3J). However, due to the small size but high density

of lipid droplets throughout the entire spheroids, those composed of 30% HUVECs exhibited the highest area of the lipid droplets per spheroid area compared to any other conditions. We also assessed the viability of cells in spheroids with or without the supplement of FFAs using a live/dead assay. The results revealed that the viability was higher than 95% for cells in spheroids regardless of the ratio of HepG2–HUVECs, indicating the supplementation of FFAs is harmless for cells for up to a week in culture. From the coculture study, we found that the analysis of colocalization of HepG2–HUVECs displayed the increased colocalization level with decreasing HUVEC ratio in spheroids (Figure 2C) as well as the level of

**ADVANCED
SCIENCE NEWS**

www.advancedsciencenews.com

**ADVANCED
BIOSYSTEMS**

www.adv-biosys.com

steatosis showed higher lipid accumulation with increasing amount of HUVECs (Figure 3I). Since the higher colocalization depicts stronger cell–cell interactions between HepG2 and HUVECs and a greater lipid area is preferable for NAFLD modeling, we propose that the NAFLD pathogenesis is better modeled when 20% of HUVECs are present to form spheroids with HepG2 cells (Figure 3L).

2.4. Steatosis Disease-on-a-Chip Model and Functionality Assessment

To examine our hypothesis regarding the bioengineering strategy to build a steatosis disease-on-a-chip model for NAFLD, we showed that 3D coculture of HepG2–HUVECs in spheroids provided a better system compared to both conventional 2D cultures and 3D cultures in the absence of HUVECs. In addition, the amount of HepG2 and HUVECs in spheroids was optimized at 20% of HUVECs and 80% of HepG2 considering both the lipid accumulation and colocalization (Figure 3L). Next, to validate the capability in building a steatosis disease model, the harvested spheroids cultured for 4 days in the inverted pyramid-shaped microwells were transferred onto a PDMS chip made by using conventional soft lithography techniques (**Figure** 4A). The chip was designed using an array of interconnected hexagonal microwells (apothem of each well: ≈150 µm; diameter of each microchannel: ≈50 µm) that recapitulate the in vivo liver physiology with each well representing a functional unit (meaning the lobule, comprising the sinusoidal units) to allow the promotion of molecular exchanges between spheroids (Figure 4B,C). The proposed design is in line with a previous study showing the architecture of networked array had the advantage of enhancing diffusion between spheroids, resulting in increases in viability and albumin secretion.[30] After transferring spheroids from the inverse pyramidal microwells to the chip, we observed that most of the wells were occupied by one spheroid (over 40%) but some of them were empty (≈24%) or filled by more than one spheroid (≈30% for two spheroids and ≈5% for three spheroids) (Figure 4D; Figure S4, Supporting Information). We speculate this may be due to several factors: 1) uneven initial seeding leading to spheroid density heterogeneity, 2) unoptimized seeding density, and/or 3) uneven surfaces along the chip (e.g., incubator, plate, or PDMS). If the transferred spheroids were shaken on a rotary shaker, the distribution bias of spheroids into the wells was more attenuated (Figure 4E). However, irrespective of the distribution of spheroids across the chips, the average number of spheroids in each well was fixed at around 1.15 (Figure 4D, inset).

To verify the possibility to induce steatosis on the chip system, spheroids (20% of HUVECs and 80% of HepG2 cells) were cultured with FFA supplementation in the wells of chips. We found that spheroids cultured for 2 days in the fatty-diet conditions showed higher levels of lipid accumulation (≈2.94-fold) compared to those cultured without the induction of FFAs (Figure 4F,G; Figures S5 and S6, Supporting Information). Long-term stability and functionality of spheroids cultured on a chip system are highly desirable for the evaluation of drugs.[31] To examine whether spheroids could be viable in long-term culture for over a week, we cultured spheroids for

9 days inside gelatin methacryloyl (GelMA) hydrogels and on the chips (Figure 4H). GelMA is known to provide a simple and inexpensive solution to culture cells in a 3D conformation by mimicking the native extracellular matrix.[32,33] Despite the long-term incubation with FFAs to maintain the steatotic state, cells cultured for 9 days were highly viable in both conditions. We also assessed the neovascularization of HUVECs inside spheroids in the presence or absence of FFAs to understand the effect of steatosis on the functionality of HUVECs (Figure 4I). Immunofluorescence images of spheroids stained with CD31 exhibited no significant differences in neovascularization between groups with and without the development of hepatic steatosis for 8 days, consistent with previous reports showing that elevated angiogenesis only appeared several weeks after disease presentation.[34,35] To examine the functionality of HepG2, we assessed the albumin secretion and reactive oxygen species (ROS) production from cells in spheroids cultured for 8 days on the chip systems (Figure 4J–M). Analysis of albumin secretion for HepG2 cultured for 8 days in spheroids displayed a continuous increase in secretion, independently of the presence of both HUVECs and FFAs, indicating that our chip system provides an ideal microenvironment for the spheroids (Figure 4J; Figure S7, Supporting Information). Furthermore, the multicellular spheroids showed higher levels of albumin secretion over 8 days compared to those without HUVECs (≈2-fold and ≈1.6-fold for without and with FFAs), which is in accordance with previous reports exhibiting cocul-turing HUVECs with hepatocytes induced increased levels of albumin secretion.[19] We also observed a notable difference of secretion in spheroids only composed of HepG2 under fat conditions (≈1.25-fold higher than those without FFAs) as shown in a previous study,[17] whereas albumin expression was not different when HUVECs interacted with HepG2 in spheroids. Analysis of the expression level of produced ROS across all conditions revealed that HepG2 cells, irrespective of the presence of HUVECs, produced higher levels of ROS in the presence of FFAs (without HUVECs: ≈1.28-fold, ≈2.43-fold, and ≈2.27-fold on days 2, 5, and 8, respectively; with HUVECs: ≈1.56-fold, ≈2.58-fold, and ≈2.14-fold on days 2, 5, and 8, respectively; the ROS intensity values of NAFLD spheroids were normalized by those from controls) than those cultured without the induction of FFAs, which is in line with previous studies showing increased ROS production with the development of steatosis (Figure 4K–M).[7] Moreover, HepG2 mixed with HUVECs in spheroids expressed higher levels of ROS (≈1.52-fold, ≈1.33-fold, and ≈1.18-fold on days 2, 5, and 8, respectively) compared to those cultured without interactions with HUVECs (Figure S8, Supporting Information). These findings suggest that our steatosis disease model—based on the 3D spheroid culture system composed of HepG2 (80%) and HUVECs (20%)—may prove to be useful in monitoring the functionality of hepatocytes while maintaining their viability to evaluate drugs.

2.5. Steatosis Reversibility and Drug Evaluation

Before evaluating drugs on our steatosis disease-on-a-chip system, we questioned whether steatosis-induced HepG2 could
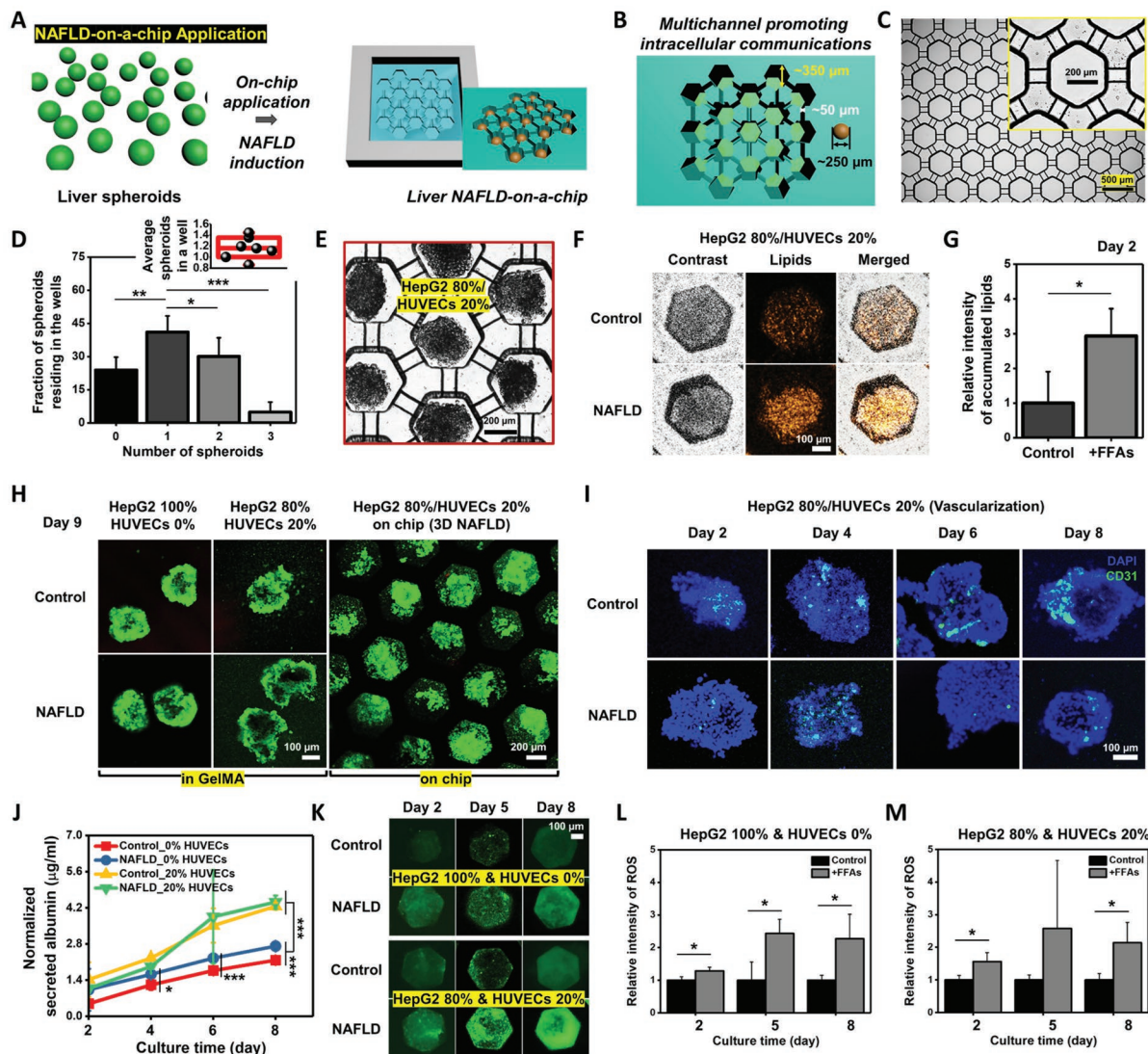
**ADVANCED
SCIENCE NEWS**

www.advancedsciencenews.com

**ADVANCED
BIOSYSTEMS**

www.adv-biosys.com

Figure 4. Development of steatosis disease model-on-a-chip system for monitoring of functionality. A) Illustrations representing NAFLD-on-a-chip application. B) Schematic displaying an array of interconnected hexagonal microwells. C) A photograph of the chip design with an apothem of each well and a diameter of each microchannel showing ≈150 and ≈50 µm, respectively. D) Fraction of spheroids residing in the interconnected wells (N = 6). The inset shows the quantification of average spheroids in the wells across the samples. E) A photograph of spheroids on chips shaken on a rotary shaker. F) Representative contrast and immunofluorescence images of spheroids on the chip stained for intracellular lipid accumulation. G) Quantification of accumulated lipids in HepG2–HUVEC spheroids cultured for 2 days on the chip (N = 4). H) Representative immunofluorescence images of live/dead staining for cells in spheroids cultured for 9 days inside GelMA hydrogels or on the chip with continuous steatosis induction. I) Representative immunofluorescence images of spheroids stained with CD31 with the presence and absence of FFAs over 8 days. J) Quantification of albumin secretion from spheroids (0% HUVECs and 20% HUVECs) with/without FFAs over 8 days (N = 4). Data were normalized according to HepG2 cell ratio. K) Representative immunofluorescence images of ROS produced from spheroids cultured for 2, 5, and 8 days on the chip. Quantification of ROS production in spheroids composed of L) 100% of HepG2 and 0% of HUVECs and M) 80% of HepG2 and 20% of HUVECs cultured for 2, 5, and 8 days on the chip with/without FFAs (N > 4 for each condition). *P < 0.05, **P < 0.005, ***P < 0.0005, Student's t-test. Error bars represent standard deviation.

be kept in the disease state or switched back to the healthy state after stopping the supplement of FFAs. Plus, if HepG2 could be returned to the healthy state, how long would it take and what role HUVECs might play in the reversal process. To answer these questions, spheroids with (20%) or without HUVECs were harvested from the inverse pyramidal microwells on day 4 and transferred to the chip system, followed by overnight stabilization on the chip. To investigate the reversibility of steatotic

HepG2, FFAs were supplemented only during the first 2 days to induce hepatic steatosis, and then, the level of lipid accumulation in spheroids with FFAs was compared to a positive control (continuous supplement of FFAs) and a negative control (without the addition of FFAs) every 2 days in healthy medium (**Figure 5**A,B). The results revealed that the level of lipids accumulated in HepG2 (positive control) could be maintained over a week independent of the presence of the HUVECs with a
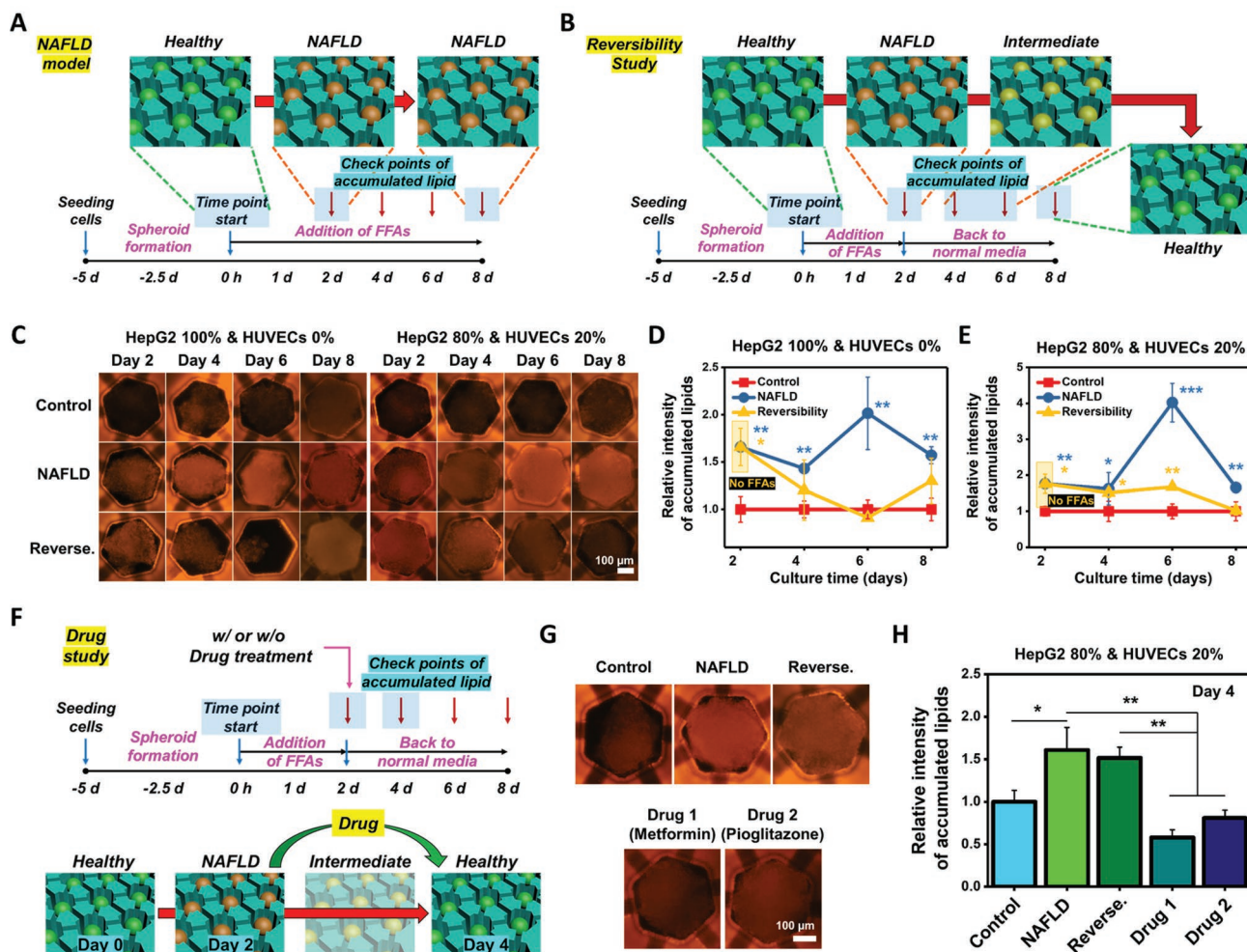
Figure 5. Steatosis reversibility and drug evaluation on NAFLD-on-a-chip system. Process flow of the experiments for A) NAFLD model and B) reversibility study. When spheroids were transferred into the microchip platform, it was considered as the experiment starting point. For NAFLD model, FFAs were continuously supplemented every 2 days of media changes, while, for reversibility, the supplement of FFAs was stopped on day 2 and cells were cultured with fresh medium without FFAs over 8 days. C) Representative immunofluorescence images of accumulated lipids over 8 days for spheroids cultured without FFAs (Control) with continuous FFA supplement (NAFLD), and with FFAs only for 2 days (Reverse). Quantification of accumulated lipids for spheroids composed of D) 100% of HepG2 and 0% of HUVECs and E) 80% of HepG2 and 20% of HUVECs cultured for 2, 4, 6, and 8 days on the chip with/without FFAs ($N > 4$ for each condition). F) Process flow of the experiments for drug study. Similar to the reversibility study, FFAs were only supplemented for 2 days in culture and antisteatotic drugs were introduced. G) Representative immunofluorescence images of accumulated lipids for spheroids cultured for 4 days with/without drugs. H) Quantification of accumulated lipids for spheroids supplemented with metformin (drug 1) or pioglitazone (drug 2) added in the culture medium with a concentration of 100×10^{-6} or 10×10^{-6} M, respectively ($N > 4$ for each condition). *$P < 0.05$, **$P < 0.005$, ***$P < 0.0005$, Student's t-test. Error bars represent standard deviation.

maximum on day 6 ($\approx$2.02-fold and $\approx$6.52-fold higher compared to the negative controls without and with HUVECs, respectively), whereas the lipid accumulation decreased to basal level (negative control) for the spheroids cultured for 8 days, which is in agreement with results previously published (Figure 5C–E).[15] Spheroids containing HUVECs delayed recovery from the steatotic state compared to those without HUVECs but finally reached basal level of intracellular lipid (on day 8). To test whether the steatosis disease-on-a-chip system could be used as a drug screening platform, we introduced antisteatotic drugs (drug 1: metformin (100×10^{-6} M); drug 2: pioglitazone (10×10^{-6} M)) to steatotic spheroids (20% of HUVECs and 80% of HepG2) on the chips (Figure 5F). Similar to the

study of reversibility, FFAs were supplemented only for 2 days and thereafter stopped, and each drug was added in the fresh healthy medium to check their effects on the level of accumulated lipids for HepG2 in spheroids. We found that steatosis could be reversed after 2 days with both drugs; lower levels of intracellular lipids were shown compared to the reversible HepG2 in spheroids without introducing drugs (metformin: $\approx$0.38-fold lower; pioglitazone: $\approx$0.54-fold lower) and even the negative control (metformin: $\approx$0.58-fold lower; pioglitazone: $\approx$0.81-fold lower) (Figure 5G,H). These findings also agree with the previous studies displaying decreased level of intracellular lipids for steatotic hepatocytes when those drugs were administered.[15,17]

ADVANCED
SCIENCE NEWS
www.advancedsciencenews.com

ADVANCED
BIOSYSTEMS
www.adv-biosys.com

3. Conclusion

To address the lack of model systems recapitulating the complex liver niche for modeling NAFLD, we developed an in vitro system based on coculturing of HepG2 and HUVECs as spheroids on chips capable of 1) modeling hepatic steatosis (the first step of NAFLD), 2) monitoring hepatic functionality, and 3) screening multiple drugs. First, the seeding density for the spheroid formation was optimized based on their morphology such as the size related to necrosis and circularity/aspect ratio. In addition, the fraction of HUVECs mixed with HepG2 as spheroids was also optimized based on the requirements of high level of 1) steatosis as well as 2) colocalization of HepG2–HUVECs. Then, we revealed that spheroids supplemented with FFAs during a culture period of 2 days turned into the steatosis stage that could be maintained for more than a week without being harmful for the cells. Analysis of the albumin secretion along with ROS production was performed to decipher the role of HUVECs inside HepG2 spheroids. Steatotic spheroids displayed similar levels of albumin and higher expression of ROS due to interactions between HepG2 and HUVECs. Furthermore, the steatosis disease-on-a-chip system was validated as a drug screening platform by demonstrating that spheroids returned back to the healthy state with faster recovery than without the use of antisteatotic drugs.

Although our study focuses more on the development of a simple but versatile system where multiple tasks (disease modeling, functionality monitoring, and drug screening) can be performed using our proposed steatosis disease-on-a-chip system, we acknowledge there are several limitations. 1) HepG2 cells that are phenotypically different from those present in human liver were employed to build the system. It is known that HepG2 cells possess a variant in the gene PNPLA3, a mutation associated with fat content that increases hepatocyte risk for steatosis and liver disease.[36] Furthermore, HepG2 cells have lower and variable CYP450 metabolism, lower levels of albumin, and ability to metabolize glucose and amino acids compared to primary hepatocytes (which use β-oxidation of fatty acids).[19,37] However, HepG2 cell line is widely used for hepatotoxicity studies and drug metabolism providing also several advantages for in vitro studies such as easy handling, low-cost, wide availability, almost unlimited lifespan, and stable phenotype.[38] We believe this issue could be addressed by employing primary hepatocytes or human induced pluripotent stem cell–derived hepatocytes, allowing better cell populations that are closer to the in vivo condition. 2) Also, other key nonparenchymal cells that are critical for disease progression were not combined to recapitulating higher levels of in vivo hepatic functionality. Nevertheless, this strategy is believed to serve as a tool to allow investigation of even more advanced stages of NAFLD by incorporating those key nonparenchymal cells presented in the liver niche for identification and validation of new drug targets for NAFLD. What is more, new potential drugs could be added to the proposed platform by combining other techniques such as 3D bioprinting, microspotting, or microarray scanning. We also expect that the suggested platform will be widely applicable across other models where cell–cell interactions play a critical role in the function and development of multicellular tissues or organs.

4. Experimental Section

Materials: All reagents and chemicals were obtained from Sigma-Aldrich, unless stated otherwise. Tissue culture plastics were obtained from Fisher Scientific. Cell culture reagents and media were obtained from Gibco.

Microfabrication of Networked Microwell Array: A networked microwell array was designed in AutoCAD (Autodesk 2018) and fabricated in a clean room using soft lithography. Briefly, a patterned (networked microwell array) master of photoresist (SU-8, MicroChem) was prepared using ultraviolet photolithography through a laser printed mask. Next, to create the patterned chips, PDMS was polymerized (1:10 ratio, cross-linker to base) on the patterned master. This chip, made of PDMS, consisted of an array of hexagonal wells of 150 µm apothem linked to each other by microchannels of 60 µm width. The chips were autoclaved for sterilization before culturing spheroids.

HepG2 and HUVEC Cell Culture: Two cell types were used in this project: HepG2 (from ATCC HB-8065) and HUVECs (from ATCC PCS-100-010). HepG2 cells were cultured in T175 flasks and maintained in a humidified incubator at 37 °C and 5% CO$_2$. The culture medium was composed of Dulbecco's modified Eagle medium (DMEM) (Gibco 11965-092, Invitrogen Co., USA) supplemented with 10% v/v fetal bovine serum (Gibco 10082, USA) and 1% penicillin–streptomycin (PS) (Fisher Scientific, Pen Strep 15140). Primary HUVECs were cultured in 1% gelatin-coated T75 flasks and maintained inside the same incubator. 10 mg of gelatin from porcine skin was dissolved per milliliter of deionized water and incubated for 5 min at 70 °C to obtain a yellow homogeneous solution. This solution was then immediately filtered using a syringe pump and a 20 µm filter. 4 mL of the solution was finally pipetted in T75 flasks and incubated at 37 °C for 1–2 h. Supernatant was removed before seeding of cells. HUVEC medium was composed of Endothelial Cell Basal Medium 2 (Promo Cell, 22011) and supplemented with Endothelial Cell Growth Medium Kit (Promo Cell, 22111). When coculturing HepG2 and HUVECs, both media were mixed together according to cell ratio.

Spheroid Formation and Culture: All spheroids were formed in microwells where each well of the culture plate (Stem Cell Technologies, AggreWell™400, 24-well plates) possesses 1200 inverted pyramid-shaped pyramidal microwells (each microwell has a diameter of 400 µm). Single cells were seeded in inverse pyramidal microwells following the protocol from Stem Cell Technologies. Briefly, 500 µL of antiadherence solution (Stem Cell Technologies, 07010) was pipetted per well of 24-well plates. The plate was centrifuged and washed with basal medium. Cells were trypsinized from culture flasks, counted, and seeded into the inverse pyramidal microwells. Medium was changed every day if cell concentration was under 0.6 million, otherwise every 12 h. Spheroids were collected after 4 days.

To transfer spheroids cultured for 4 days in the inverse pyramidal microwells into the chips, a 1 mL pipette was used to gently collect the spheroids (spheroids can be detached by gentle pipetting) and seed them onto the networked microwell array. The transferred spheroids were shaken on a rotary shaker for 10 min for the better distribution.

Cell Tracking in Spheroids: Two different cell trackers, CM-Dil (Invitrogen, CellTracker Red C7001) and CMFDA (Invitrogen, CellTracker Green C2925), were used to observe the location of HepG2 and HUVECs, respectively. The protocols were furnished by the manufacturer. For the red dye, stock solution was first prepared in dimethyl sulfoxide (DMSO) at 1 mg mL^{-1} and then diluted 1000× in phosphate-buffered saline (PBS, working solution). HepG2 were trypsinized from tissue culture dishes and then incubated in the working solution for 5 min or less at 37 °C, followed by an additional 15 min at 4 °C. After labeling, the cells were washed with PBS and resuspended in fresh medium. For the green dye, stock solution was prepared in DMSO at a final concentration of 5×10^{-3} M and then diluted 1000× in serum-free medium (working solution). HUVECs were also trypsinized from culture flasks and introduced in the warmed working solution and incubated for 20 min. The cells were then centrifuged, and the working solution was removed. Cells were finally resuspended in fresh medium. These

cells labeled with the fluorescence dyes were seeded onto the inverse pyramidal microwells. After spheroid formation, HepG2 and HUVECs were visualized using a confocal microscope (LSM880; Zeiss).

Immunofluorescence: Cells were washed two times with PBS and fixed using 4% paraformaldehyde for 20 min at room temperature (RT). Cells were washed three times with PBS with 3 min incubation at RT between each washing step. For membrane permeabilization, 0.1% Triton X-100 (in PBS, permeabilization buffer) was added to cells for 20 min at RT, followed by washing them two times with PBS with 3 min of incubation at RT between each washing step. For blocking, BSA was added to the permeabilized cells for 5 min at RT. DAPI (1:1000) and phalloidin (Invitrogen, 1:200) were diluted in PBS. The final solution was pipetted in the samples and incubated for 20 min at 37 °C. Cells were washed three times with PBS (5 min incubation at RT between each washing step). Stained cells were observed under fluorescence (Zeiss Axio Observer; Zeiss) or confocal microscope.

Biochemical Assay: For biochemical assay, culture medium was first removed, and cells were then washed with warm PBS (to remove phenol red in the media). Live/dead staining solution was added to cells with the following ratio: 2 μL ethidium homodimer and 0.5 μL calcein AM in 1 mL PBS. Cells were incubated for 15–20 min at 37 °C followed by washing them two times with PBS. Cells were observed under fluorescence or confocal microscope.

Steatosis Induction: Two FFAs were used to induce steatosis: palmitic acid (Sigma-Aldrich, USA, P0500-10G) and oleic acid (Sigma-Aldrich, USA, O1383-5G). Steatosis was induced following a previously described method.[14] Briefly, 0.33 M of PA and 0.66 M of OA were dissolved in methanol, and this solution was diluted 1000× in cell media (final working concentration: 0.33×10^{-3} M PA and 0.66×10^{-3} M OA). Cells transferred from inverse pyramidal microwells or seeded in multiwell plates were cultured overnight in healthy medium (DMEM supplemented with 10% FBS and 1% PS). FFAs in DMEM supplemented with 10% FBS and 1% BSA (Sigma) were added to cells, and the FFA-supplemented medium was replaced every 2 days.

Evaluation of Intracellular Lipid Accumulation: Intracellular lipid accumulation was evaluated using AdipoRed assay (Lonza, Walkersville, USA, PT-7009) for cells cultured on multiwell plates or chips according to the manufacturer's instructions. Cells on multiwell plates or chips were washed with PBS. Solution of AdipoRed dye was added to PBS (30 μL mL^{-1}) and pipetted to each well. Lipid accumulation was quantified using a fluorescence or confocal microscope.

Reactive Oxygen Species Production: Stock solution of carboxy-H2DCFDA (general oxidative stress indicator, Thermo Fisher Scientific, C400) was dissolved in DMSO at a concentration of 10×10^{-3} M and stored at −80 °C. Working solution was prepared by dissolving stock solution in PBS at a final concentration of 10×10^{-6} M. ROS production was assessed according to manufacturer's instructions. Samples with the working solution were washed with PBS and incubated for 30–60 min at 37 °C. The dye solution was then replaced by PBS with 10% FBS, and the level of ROS produced from cells was observed using a confocal fluorescence microscope.

Albumin Secretion: Albumin Human ELISA Kit (Invitrogen, USA) was used to measure the level of albumin present in the culture medium according to manufacturer's instructions. Cell culture medium was collected every 2 days and frozen at −80 °C until use. Two experimental and technical replicates (total four replicates) were used to assess intravariability and intervariability, respectively. The assay was evaluated at 450 and 550 nm using the plate reader (BIOTEK fluorescent plate reader, Synergy HTX multimode reader). Absorbance values were read three times and averaged before subtracting 450 to 550 nm values. Samples containing cell culture media were diluted two times to create the standard curve. Albumin concentration values were normalized according to HepG2 cell ratio.

Drug Study: Metformin hydrochloride and pioglitazone hydrochloride (Sigma-Aldrich) were used as antisteatotic drugs. Both were dissolved in DMSO (stock solution of 100×10^{-3} and 10×10^{-3} M, respectively). Stock solutions were dissolved in cell culture medium in a working concentration of 100×10^{-6} and 10×10^{-6} M, respectively.

Image Collection, Processing, and Analysis: Photographs of spheroids cultured for 4 days in the inverse pyramidal microwells were obtained using a fluorescence microscope (bright field, Zeiss Axio Observer; Zeiss). The characterization of spheroid shape (diameter, circularity, and aspect ratio) was performed setting first the scale (pixel to micrometer conversion) using ImageJ (Fiji). A Gaussian filter was used to blur the image facilitating the spheroid edge detection (typical sigma radius between 3 and 7). The image was then converted to a mask. Finally, parameters can be obtained using Analyze Particles. Immunofluorescence microscopy was conducted using a confocal microscope (LSM880; Zeiss) or fluorescence microscope (Zeiss Axio Observer; Zeiss). ImageJ was also used for the quantification of images collected from both fluorescence and confocal microscopes. Spheroids were imaged for each condition and their fluorescence intensities were used to compare the expression of ROS or AdipoRed dye. Specifically, background intensities of raw fluorescence images were subtracted, and intensities from multiple regions in each spheroid were averaged to compare with others. Intensities from spheroids with the FFA induction were normalized by those from spheroids without the supplement.

Statistics: For morphology and intensity analysis including colocalization, lipid accumulation, and ROS, images were used without any preprocessing. Data were obtained from three replicates, confirmed by at least three independent experiments, and expressed as the mean ± standard deviation unless otherwise specified. ANOVA analysis (http://statpages.info/anova1sm.html) was performed. $P < 0.05$ was considered statistically significant.

Supporting Information

Supporting Information is available from the Wiley Online Library or from the author.

Acknowledgements

Conflict of Interest

The authors declare no conflict of interest.

Keywords

[1] Z. Kmieć, *Cooperation of Liver Cells in Health and Disease (Advances in Anatomy Embryology and Cell Biology)*, Vol. **161**, Springer: Berlin **2001**.

[2] K. Vekemans, F. Braet, *World J. Gastroenterol.* **2005**, *11*, 5095.

[3] E. M. Brunt, V. W.-S. Wong, V. Nobili, C. P. Day, S. Sookoian, J. J. Maher, E. Bugianesi, C. B. Sirlin, B. A. Neuschwander-Tetri, M. E. Rinella, *Nat. Rev. Dis. Primers* **2015**, *1*, 15080.

[4] Z. Younossi, Q. M. Anstee, M. Marietti, T. Hardy, L. Henry, M. Eslam, J. George, E. Bugianesi, *Nat. Rev. Gastroenterol. Hepatol.* **2017**, *15*, 11.

[5] N. L. Gluchowski, M. Becuwe, T. C. Walther, R. V. Farese, *Nat. Rev. Gastroenterol. Hepatol.* **2017**, *14*, 343.

[6] M. Benedict, X. Zhang, *World J. Hepatol.* **2017**, *9*, 715.

[7] E. Buzzetti, M. Pinzani, E. A. Tsochatzis, *Metabolism* **2016**, *65*, 1038.

[8] S. L. Friedman, B. A. Neuschwander-Tetri, M. Rinella, A. J. Sanyal, *Nat. Med.* **2018**, *24*, 908.

[9] B. K. Cole, R. E. Feaver, B. R. Wamhoff, A. Dash, *Expert Opin. Drug Discovery* **2018**, *13*, 193.

[10] J. T. Haas, S. Francque, B. Staels, *Annu. Rev. Physiol.* **2016**, *78*, 181.

[11] L. Hebbard, J. George, *Nat. Rev. Gastroenterol. Hepatol.* **2011**, *8*, 35.

[12] Y. Takahashi, *World J. Gastroenterol.* **2012**, *18*, 2300.

[13] E. W. Esch, A. Bahinski, D. Huh, *Nat. Rev. Drug Discovery* **2015**, *14*, 248.

[14] M. Gori, M. C. Simonelli, S. M. Giannitelli, L. Businaro, M. Trombetta, A. Rainer, *PLoS One* **2016**, *11*, e0159729.

[15] M. Kozyra, I. Johansson, Å. Nordling, S. Ullah, V. M. Lauschke, M. Ingelman-Sundberg, *Sci. Rep.* **2018**, *8*, 14297.

[16] I. Cordero-Herrera, M. Kozyra, Z. Zhuge, S. McCann Haworth, C. Moretti, M. Peleli, M. Caldeira-Dias, A. Jahandideh, H. Huirong, J. C. Cruz, A. L. Kleschyov, M. F. Montenegro, M. Ingelman-Sundberg, E. Weitzberg, J. O. Lundberg, M. Carlstrom, *Proc. Natl. Acad. Sci. USA* **2019**, *116*, 217.

[17] T. Kostrzewski, T. Cornforth, S. A. Snow, L. Ouro-Gnao, C. Rowe, E. M. Large, D. J. Hughes, *World J. Gastroenterol.* **2017**, *23*, 204.

[18] S. Y. Lee, J. H. Sung, *Biotechnol. Bioeng.* **2018**, *115*, 2817.

[19] C. H. Beckwitt, A. M. Clark, S. Wheeler, D. L. Taylor, D. B. Stolz, L. Griffith, A. Wells, *Exp. Cell Res.* **2018**, *363*, 15.

[20] G. G. Y. Chiew, A. Fu, K. Perng Low, K. Qian Luo, *Sci. Rep.* **2015**, *5*, 10801.

[21] A. Ehrlich, S. Tsytkin-Kirschenzweig, K. Ioannidis, M. Ayyash, A. Riu, R. Note, G. Ouedraogo, J. Vanfleteren, M. Cohen, Y. Nahmias, *Lab Chip* **2018**, *18*, 2510.

[22] R. E. Feaver, B. K. Cole, M. J. Lawson, S. A. Hoang, S. Marukian, B. R. Blackman, R. A. Figler, A. J. Sanyal, B. R. Wamhoff, A. Dash, *JCI Insight* **2016**, *1*, e90954.

[23] B. Patra, Y.-S. Peng, C.-C. Peng, W.-H. Liao, Y.-A. Chen, K.-H. Lin, Y.-C. Tung, C.-H. Lee, *Biomicrofluidics* **2014**, *8*, 052109.

[24] N. S. Bhise, V. Manoharan, S. Massa, A. Tamayol, M. Ghaderi, M. Miscuglio, Q. Lang, Y. Shrike Zhang, S. R. Shin, G. Calzone, N. Annabi, T. D. Shupe, C. E. Bishop, A. Atala, M. R. Dokmeci, A. Khademhosseini, *Biofabrication* **2016**, *8*, 014101.

[25] H. Gaskell, P. Sharma, H. E. Colley, C. Murdoch, D. P. Williams, S. D. Webb, *Toxicol. Res.* **2016**, *5*, 1053.

[26] T. Kietzmann, *Redox Biol.* **2017**, *11*, 622.

[27] R. Gebhardt, *World J. Gastroenterol.* **2014**, *20*, 8491.

[28] G. J. van der Vusse, *Drug Metab. Pharmacokinet.* **2009**, *24*, 300.

[29] M. A. Munteanu, G. A. Nagy, P. A. Mircea, *Clujul Med.* **2016**, *89*, 19.

[30] G. H. Lee, J. S. Lee, G.-H. Lee, W. Y. Joung, S. H. Kim, S. H. Lee, J. Y. Park, D.-H. Kim, *Biofabrication* **2017**, *10*, 015001.

[31] K. Moshksayan, N. Kashaninejad, M. E. Warkiani, J. G. Lock, H. Moghadas, B. Firoozabadi, M. S. Saidi, N.-T. Nguyen, *Sens. Actuators, B* **2018**, *263*, 151.

[32] J. W. Nichol, S. T. Koshy, H. Bae, C. M. Hwang, S. Yamanlar, A. Khademhosseini, *Biomaterials* **2010**, *31*, 5536.

[33] B. J. Klotz, D. Gawlitta, A. J. W. P. Rosenberg, J. Malda, F. P. W. Melchels, *Trends Biotechnol.* **2016**, *34*, 394.

[34] M. Miyao, H. Kotani, T. Ishida, C. Kawai, S. Manabe, H. Abiru, K. Tamaki, *Lab. Invest.* **2015**, *95*, 1130.

[35] F. J. Gonzalez-Paredes, G. H. Mesa, D. M. Arraez, R. M. Reyes, B. Abrante, F. Diaz-Flores, E. Salido, E. Quintero, M. Hernández-Guerra, *PLoS One* **2016**, *11*, e0156650.

[36] C. J. Green, D. Johnson, H. D. Amin, P. Sivathondan, M. A. Silva, L. M. Wang, L. Stevanato, C. A. McNeil, E. A. Miljan, J. D. Sinden, K. J. Morten, L. Hodson, *Am. J. Physiol. Endocrinol. Metab.* **2015**, *309*, E511.

[37] J. R. Wiśniewski, A. Vildhede, A. Norén, P. Artursson, *J. Proteomics* **2016**, *136*, 234.

[38] *Protocols in In Vitro Hepatocyte Research (Methods in Molecular Biology)* (Eds: M. Vinken, V. Rogiers), Humana Press, New York **2015**.